ELSEVIER

Journal of Nuclear Materials 251 (1997) 262–268

journal of nuclear materials

Low temperature mechanical properties of steels containing high concentrations of helium

H. Ullmaier [a], E. Camus [b,*]

[a] *Institut für Festkörperforschung des Forschungszentrums Jülich, D-52425 Jülich, Germany*
[b] *Hahn-Meitner-Institut Berlin GmbH, Glienicker Strasse 100, D-14109 Berlin, Germany*

Abstract

Results of tensile tests and hardness measurements in the temperature range 25–400°C are reported for ferritic–martensitic steels and s.a. 316 L austenitic steel. Helium concentrations up to 1 at.% have been introduced into these materials by α-particle (0–25 MeV) implantation and He/Fe dual-beam (15/300 keV) irradiation, respectively. In the latter case displacement damage up to 50 dpa was produced simultaneously with the introduction of He. From a preliminary analysis of the results and a comparison with earlier data it may be concluded that for temperatures up to at least 400°C the observed hardening is dominated by displacement damage. Only for very high helium concentrations around 1 at.% a moderate further increase of hardness is found, indicating that helium does not have a drastic effect on the mechanical properties of the investigated alloys. © 1997 Elsevier Science B.V.

1. Introduction

In spallation neutron sources, the target materials and the structural materials which are in or close to the proton beam are subject to extremely high helium production rates. This is illustrated by the so-called He/dpa ratio, a parameter which is used to indicate the relative importance of helium effects in nuclear materials: for steels the He/dpa ratios are 0.5, 15 and 200 appm/dpa for fast fission, fusion and spallation, respectively. Even more alarming are the high absolute values of the He production: in the proton window of ESS, the planned 5 MW European Spallation Source [1], about 1 at.% He will be accumulated within one year of operation (together with about 50 dpa) [2].

A recently completed feasibility study for ESS [1] identified a liquid mercury target as the optimum choice and this concept was also adopted in the USA for the design of the National Spallation Neutron Source (NSNS) [3]. In this case the operating temperatures of structural target components (Hg container, flow guides, return vessel, proton beam windows) will lie between room temperature and 300°C, a range of minor importance for fusion materials research where helium effects are intensively investigated. It is thus not surprising that data on the influence of high concentrations at temperatures below 300°C are very scarce.

The most important way to build up a data base for the behaviour of materials in a spallation environment is the investigation of spent targets and target components from existing medium power sources (ISIS in UK and LAMPF in USA). Preliminary first results have been reported recently [4]. Complementary to these efforts, simulation experiments employing light and heavy ions have been started. In this contribution we report first results of tensile tests and hardness measurements for ferritic–martensitic steels and an austenitic steel, which had been implanted with up to 1 at.% He. These materials are considered as prime candidates for structural components in ESS and NSNS [1,3].

2. Experimental

2.1. 25 MeV α-particle implantations

Miniature tensile specimens (0.1 mm thickness, 10 mm and 3 mm gauge length and width, respectively) were prepared from the ferritic–martensitic steel Manet and the

* Corresponding author. Tel.: +49-30 8062 2761; fax: +49-30 8062 2824; e-mail: camus@hmi.de.

PII S0022-3115(97)00226-2

austenitic steel AISI 316 L. Both steels are reference materials of the European Fusion Programme and their specifications can be found in Refs. [5,6], respectively. After preparation, the Manet specimens were heated to 1075°C for 30 min, quenched and finally tempered at 700°C for 2 h. The 316 L specimens were solution annealed at 1050°C for 2 h. All heat treatments were performed in vacuum. One part of the specimens served as reference specimens, the other part was attached to water-cooled copper blocks by low temperature solder (melting point 70°C). Each block containing two specimens was inserted into an irradiation chamber at the Jülich Compact Cyclotron and exposed to an α-beam with 25 MeV initial energy. Before entering the specimens, the α-particles passed Al foils of varying thickness which were mounted on the circumference of a degrader wheel. In this way the implantation energy was varied between 0 and 25 MeV, resulting in a homogeneous loading of the specimen thickness. Lateral uniformity was achieved by wobbling the beam in x and y directions. Typical implantation rates were around 100 appm/h.

After implantation to about 0.5 at.% He (resulting in a concurrent displacement damage of 0.5 dpa) the specimens were tensile tested in vacuum at temperatures of 25, 150 an 300°C, respectively (strain rate $\approx 10^{-4}$ s^{-1}). Thorough investigations [7] have shown that tensile data from foil specimens and standard specimens agree rather well. Agreement is most perfect for the yield stress $\sigma_{0.2}$, while the ultimate tensile strength σ_{UTS} and especially the fracture strain ε_F sometimes deviate in both directions. We therefore use the strain to necking, ε_{STN}, instead of ε_F, for characterizing the ductility of the materials.

After tensile testing, the fracture surfaces of the specimens were observed by SEM and Vickers hardness HV was measured using loads L between 1 and 5 N. We have used the definition HV = L/A_p, where A_p is the projected contact area along the indentation axis between indenter and specimen. The hardness increase ΔHV was determined as the difference of the HV-values in the implanted gauge section and the HV-values in the unirradiated and unstrained shoulders of the specimens. Finally, disks of 3 mm in diameter were punched out of the gauge sections and the shoulders, respectively, for future TEM analysis of the irradiation-induced microstructural changes.

The simulation method described in this section has the advantage of providing homogeneously loaded specimen volumes sufficient for tensile testing, i.e., mechanical properties of direct engineering relevance can be obtained. On the other hand, the displacement damage produced during the implantation is only about 1 dpa per at.% He as compared to about 100 dpa per at.% He in the spallation case. A further drawback is the relatively small implantation rate of about 100 appm/h (with a concurrent damage rate of about 2×10^{-6} dpa/s) which severely limits the number of implanted specimens due to restrictions in cyclotron beam time.

2.2. 15 keV He / 300 keV Fe dual-beam irradiations

Specimens of the Japanese steel F82H mod were irradiated at the dual-beam facility of the Hahn-Meitner-Institut Berlin. This alloy is a low activation ferritic–martensitic steel which is under consideration for the Fusion Program as well as for the European Spallation Source as structural material. Its specifications can be found in Ref. [8]. The alloy was delivered in the normalized-and-tempered condition (1040°C for 37 min/quenched/750°C for 1 h) very similar to that of the Manet steel. Thin sheets (typically 100 μm) were cut from the delivered ingots. The specimens (3 mm discs) were then punched out from the sheets, polished electrolytically, and finally irradiated. Irradiations with 300 keV Fe^+ ions and simultaneous implantation with 15 keV He^+ ions were performed. The specimen holder is a commercial TEM holder allowing irradiations to be performed in a wide temperature range. The current densities of both beams were chosen to produce the He/dpa ratio of 200 appm/dpa typical for the spallation environment. Displacement and implantation rates as high as 10^{-2} dpa/s and 10 appm/s can be reached allowing to introduce high damage levels and high helium concentrations within a few hours. In the present study, the specimens were irradiated up to a dose of 50 dpa and a helium content of 1 at.%.

The main drawback of this kind of ion irradiation is that only a small volume of the sample can be damaged. 300 keV Fe^+ ions have a penetration depth of typically 100 nm below the specimen surface. Information on the changes of mechanical properties of the alloy can therefore be deduced from nanohardness measurements only. The measurements were carried out with a Nano Indenter II of Nano Instrument, Oak Ridge, USA [9]. Indentations were performed with a Berkovitch indenter using loads L smaller than 8 mN. The nanohardness HN was also defined by HN = L/A_p.

3. Results

3.1. Ferritic–martensitic steels

Tensile tests at 25, 150 and 300°C, respectively, have been performed on Manet specimens which had been homogeneously implanted with 0.55 at.% He (≈ 0.55 dpa). Fig. 1 shows two typical stress–strain curves together with the pertinent reference curves. From the stress–strain curves the yield stress $\sigma_{0.2}$, the ultimate tensile strength σ_{UTS} and the strain to necking ε_{STN} are obtained and plotted in Fig. 2 for the three test temperatures. The irradiation-induced increase in yield stress of $\Delta\sigma_{0.2} \approx 420$ MPa is practically independent of temperature. A comparison with earlier results [11,12] on the same material (Fig. 3) shows that the data obey the empirical relation $\Delta\sigma_{0.2} = AK^{1/3}$ where A is a material-dependent constant and K is the displacement dose.

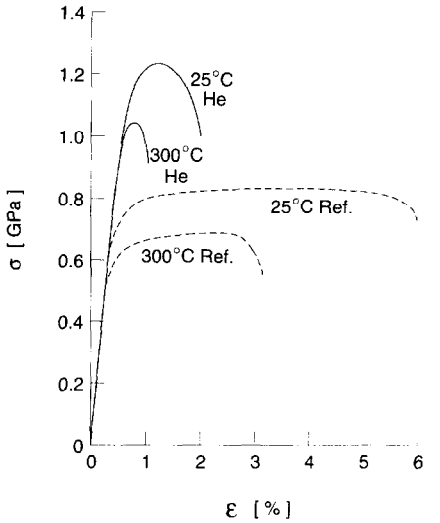

Fig. 1. Stress–strain curves of Manet steel at 25 and 300°C, respectively. The dotted curves refer to the reference specimens, the solid lines give the tensile behaviour of specimens implanted with 0.55 at.% He (≈ 0.55 dpa, 2×10^{-6} dpa/s).

SEM observation of the fracture regions revealed chisel-type reductions in area which decreased with decreasing fracture strain. The fracture surfaces remained ductile and transgranular even for the specimen with lowest ductility, i.e., for the case 0.55 at.% He (0.55 dpa) and

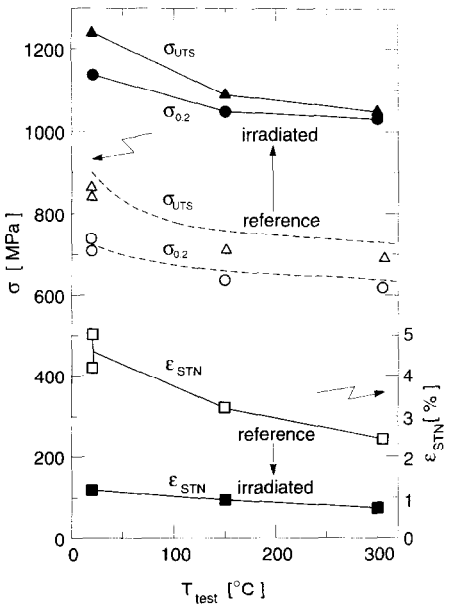

Fig. 2. Yield stress $\sigma_{0.2}$, ultimate tensile strength σ_{UTS}, and strain to necking ε_{STN}, as a function of test temperature for Manet. The open symbols refer to reference specimens, the closed symbols to specimens implanted with 0.55 at.% He (≈ 0.55 dpa, 2×10^{-6} dpa/s). The dotted lines refer to reference data given in Ref. [10].

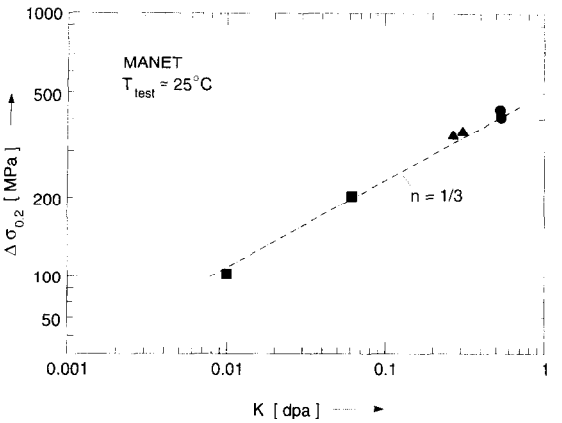

Fig. 3. Increase in yield stress $\Delta\sigma_{0.2}$ of irradiated (implanted) Manet specimens as a function of the displacement dose K. The tensile test temperature was around 25°C. Data from (■) H/He implantation ($\approx 10^{-7}$ dpa/s to 2×10^{-6} dpa/s) [11], (▲) 590 MeV proton irradiation [12], (●) this work ($\approx 2\times10^{-6}$ dpa/s).

$T_{test} = 300$°C where $\varepsilon_{STN} = 0.8\%$. It is worth mentioning that the angle between fracture surface and load axis was $30 \pm 1°$ for all specimens tested.

Nanohardness measurements have been performed on dual-beam implanted (Fe + He) and single beam irradiated (Fe) specimens. Fig. 4 shows two typical nanohardness curves. The nanohardness is plotted as a function of indentation depth. The method of continuous stiffness measurement (CSM) was employed to record continuously the hardness as a function of depth [9]. Each data point is the mean value of typically 10 individual indentations. The given error bars correspond to 1 standard deviation. In the

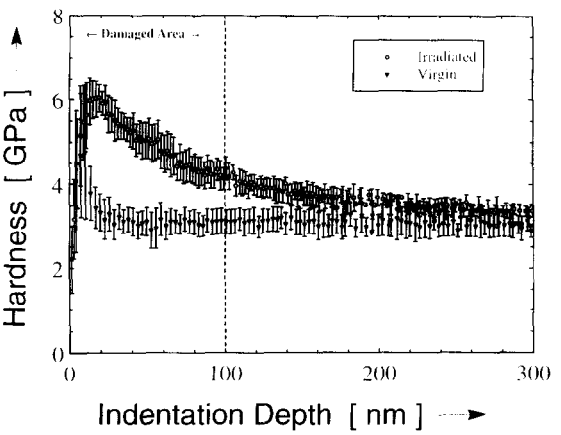

Fig. 4. Nanohardness HN as a function of indentation depth d for F82H specimens dual-beam irradiated at 113°C to 50 dpa/1 at.% He (open symbols) and unirradiated (filled symbols). The difference between the peak values of the curves for irradiated and reference specimens, respectively, is taken as representative for the hardness increase and is plotted in the right part of Fig. 5.

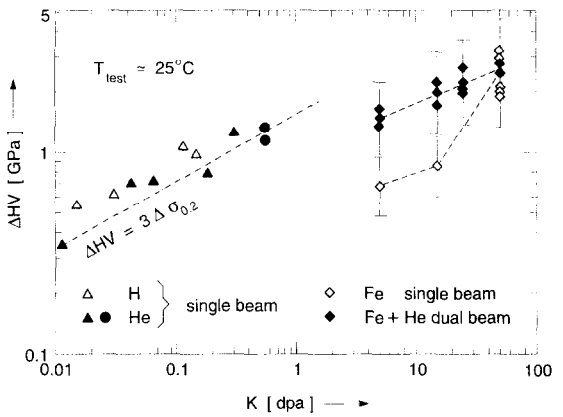

Fig. 5. Increase in hardness ΔHV of irradiated (implanted) Manet specimens as a function of the displacement dose K, obtained from microhardness measurements on H/He implanted specimens (Δ▲ H/He implanted [14], ● this work, displacement rate 1 to 3.5×10^{-6} dpa/s) and nanohardness measurements (◇◆ dual-beam irradiated, this work), respectively. The F82H mod specimens were implanted and/or irradiated at temperatures between 113°C and 400°C with rates of 5 appm He/s and 2.5×10^{-2} dpa/s. The dash-dotted line indicates an empirical relation between yield stress and hardness increase using $\Delta\sigma_{0.2}$ values of Fig. 3. The dotted lines connecting the dual-beam data have no physical meaning and serve as eye guides only.

first 10 nm below the surface, the hardness increases very rapidly and reaches a maximum at a depth of 15 to 20 nm, which is about one seventh of the thickness of the irradiated region. At deeper depths, nonirradiated regions start to contribute to the measurement, resulting in a decrease of the hardness. At depths of 250 to 300 nm, the hardness approaches a constant value which is equal to the value for the reference specimens. In the following, the peak hardness value is taken as representative of the irradiated volume.

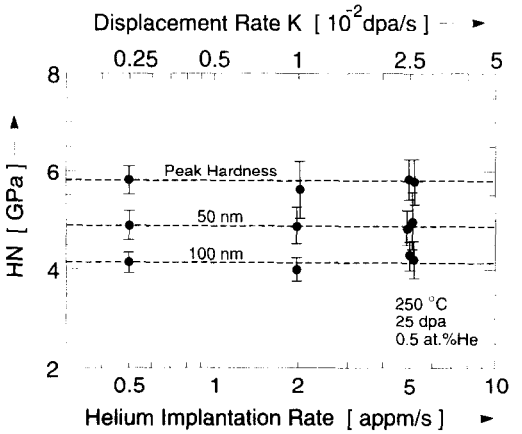

Fig. 6. Nanohardness HN at different indentation depths as a function of displacement or implantation rate in F82H mod specimens dual-beam irradiated at 250°C to 25 dpa and implanted with 0.5 at.% He, respectively.

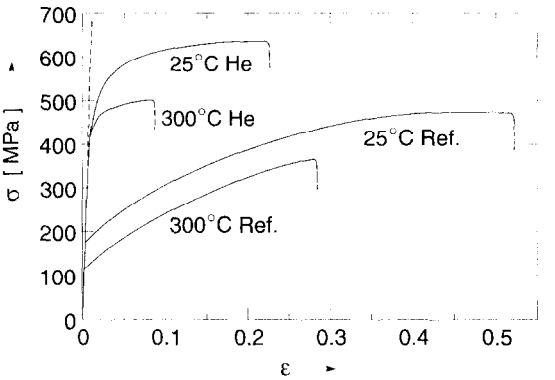

Fig. 7. Stress–strain curves of 316 L steel at 25 and 300°C, respectively. The curves labelled He refer to specimens implanted with 0.45 at.% He (≈ 0.45 dpa, 2×10^{-6} dpa/s).

The results of Vickers hardness measurements performed after the tensile tests are shown in Fig. 5, together with earlier data [13] on the same material and with nanohardness results on F82H mod steel irradiated to high doses at temperatures between 113°C and 400°C. At low doses, the data for the hardness increase ΔHV scatter around the empirical relation $\Delta H = 3\Delta\sigma_{0.2}$ (dash-dotted line in Fig. 5) which is often used to correlate tensile and hardness data.

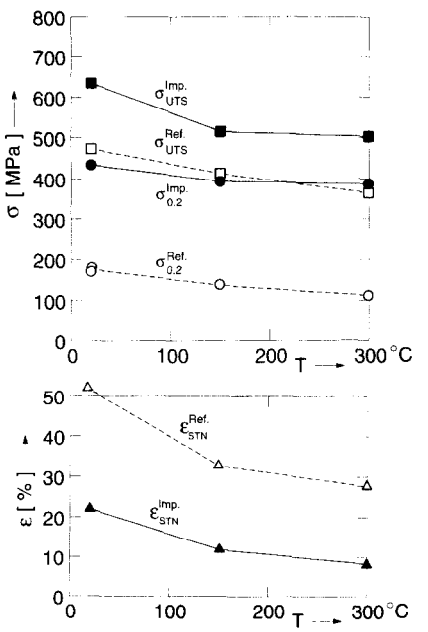

Fig. 8. Yield stress $\sigma_{0.2}$, ultimate tensile strength σ_{UTS}, and strain to necking ε_{STN} as a function of test temperature for 316 L. The open symbols refer to reference specimens, the closed symbols to specimens implanted with 0.45 at.% He (≈ 0.45 dpa, 2×10^{-6} dpa/s).

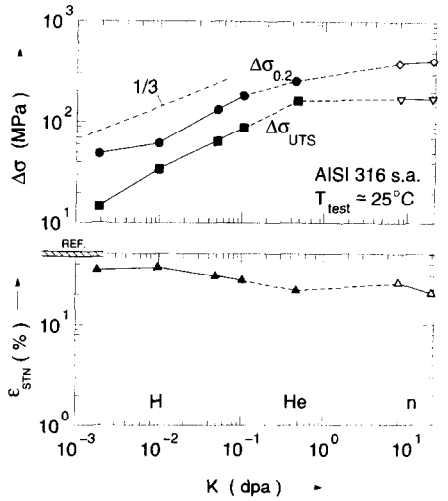

Fig. 9. Increase in yield stress $\Delta\sigma_{0.2}$ and ultimate tensile strength $\Delta\sigma_{UTS}$, and strain to necking ε_{STN}, respectively, at 25°C as a function of displacement dose K. The closed symbols refer to H/He implantations ($\approx 10^{-7}$ dpa/s to 2×10^{-6} dpa/s), the open symbols are neutron data [11].

Apart from the different test methods (HV vs. HN), the two sets of data in Fig. 5 were obtained by different implantation or displacement rates. We therefore investigated their possible influence by varying the rates to reach a given damage level. Fig. 6 displays the nanohardness at different depths as a function of the implantation or displacement rate for a He concentration of 0.5 at.%. Within the experimental uncertainty, the hardness is independent of the rates which suggests that plotting of cyclotron data

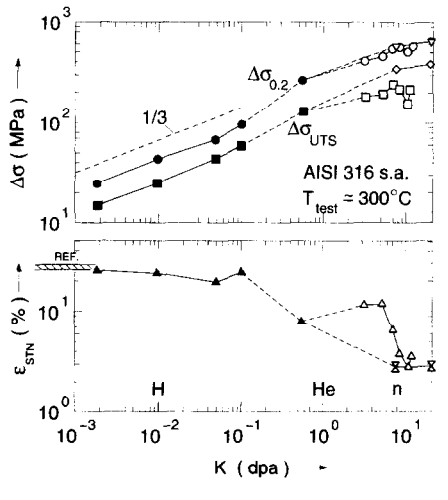

Fig. 10. Increase in yield strength $\Delta\sigma_{0.2}$ and ultimate tensile strength $\Delta\sigma_{UTS}$, and strain to necking ε_{STN}, respectively, at 300°C as a function of displacement dose K. The closed symbols refer to H/He implantations ($\approx 10^{-7}$ dpa/s to 2×10^{-6} dpa/s), the open symbols are neutron data [11,12].

and dual-beam data in a common graph (Fig. 5) is reasonable.

3.2. Austenitic steel

Tensile tests at 25, 150 and 300°C, respectively, have been performed on solution annealed 316 L specimens which had been homogeneously implanted with 0.45 at.% He (≈ 0.45 dpa). Fig. 7 shows two typical stress–strain curves with the pertinent reference curves. The temperature dependences of the corresponding $\sigma_{0.2}$, σ_{UTS} and ε_{STN} values are given in Fig. 8. A compilation of literature data on tensile parameters after irradiation with protons [14] and neutrons [15,16] is given in Figs. 9 and 10 for test temperatures around 25°C and 300°C, respectively. As for the case of the martensitic steel, the increase of the yield stress, $\Delta\sigma_{0.2}$, follows a $K^{1/3}$-dependence at low doses. The ductility is only little degraded by irradiation. For the case 0.45 at.% He (0.45 dpa) and $T_{test} = 300$°C, $\varepsilon_{STN} = 8\%$, as compared to 0.8% for the martensitic steel. It is therefore not astonishing that SEM observation of the fracture surfaces points to ductile and transgranular failure of all 316 L specimens tested.

4. Discussion

The main aims of the present investigation were

(1) To get information on the evolution of mechanical properties of specimens irradiated at high doses (50 dpa) and containing high concentrations of helium (1 at.%). One challenge was to find out whether results from hardness tests (especially from nanohardness measurements on dual-beam irradiated specimens) can yield information on bulk mechanical properties. The dual-beam simulation technique is the only method which can provide high dose data with spallation-relevant He/dpa ratios in short lengths of time. If the method were applicable at least for screening, the materials selection would be greatly facilitated.

(2) To obtain a first experimental confirmation of the expectation that helium is at low temperatures ($T < 0.3$ of melting temperature T_M) less detrimental to the mechanical properties than at $T > 0.45T_M$ where strong helium embrittlement [17] is observed. If helium were indeed of minor importance, the reliability of lifetime estimates for spallation target components [18] based on fission and fusion data [15,16,19–21] could be significantly improved.

4.1. Relevance of nanohardness data

The hardness evolution in the F82H mod steel at high doses was deduced from specimens irradiated to a depth of only 100 nm. The relevance of the nanohardness tests for information on bulk properties must therefore be addressed.

Recent results on a comparison of nanohardness HN and Vickers hardness HV on bulk specimens [22] suggest a relation $\Delta HN = 1.1\Delta HV$, where ΔHV was defined as the ratio L/A_c, A_c being the contact area between indenter and specimen. The proportionality constant is very close to the geometrical factor of $A_c/A_p = (\sin(\Phi/2))^{-1} = 1.078$ ($\Phi = 136°$), which accounts for the different definitions of HN and HV. This indicates that ΔHN values can indeed be directly and quantitatively compared to ΔHV bulk values.

For all temperatures lower than 400°C, the dual-beam irradiated specimens show, after 50 dpa and 1 at.% He irradiation, hardness values which amount to approximately 1.7 times the nonirradiated value. Similar increases in hardness were also observed in austenitic and ferritic–martensitic steels irradiated at 200°C and 350°C at the triple-beam accelerator of the Oak Ridge National Laboratory, USA, using charged particles (4 MeV Fe^{2+}, 400 keV He^+, 200 keV H^+) of much higher energies than in the present work [23]. This indicates that our nanohardness measurements performed on dual-beam implanted specimens may be considered as to be quantitative.

The measurements carried out on the specimens irradiated only with Fe reveal a much smaller hardness increase after an irradiation to 5 or 15 dpa. This effect is probably an artefact due to the presence of the specimen surface. The surface acts as an extended sink and annihilates the defects produced during the irradiation thus reducing the magnitude of the hardening. The reason why this artefact does not appear in the case of the dual-beam irradiation is probably the presence of helium-vacancies complexes and/or helium bubbles in the latter case. The presence of gas bubbles will result in an increase of the effective sink strength of the specimen and hence reduce or even suppress the influence of the surface [1].

4.2. Dose and helium concentration dependence of hardening

An indication of the relative importance of displacement defects and helium, respectively, on hardening is obtained from Figs. 3, 5, 9 and 10. They include data of this work and earlier results and show a good correlation with the displacement dose K, rather independent of the type and energy of the different irradiating particles having widely varying He/dpa ratios. At low doses and low helium concentrations, the changes in yield stress, ultimate tensile strength and Vickers hardness in both types of steels increase with $K^{1/3}$ which is often found for irradiation-induced hardening of alloys. For doses above ≈ 1 dpa, the tensile parameters and the hardness tend to saturation as expected. Attempts to establish analogous correlations with the helium concentration failed.

[1] For a quantitative analysis, see for example Ref. [24].

This finding together with the negligible dependence of the hardness changes on temperature (Figs. 2 and 8) and dose rate (Fig. 6) suggests that for temperatures up to 400°C, doses smaller than ≈ 1 dpa, and helium concentration smaller than $c_{He} \approx 0.5$ at.%, the observed strengthening is also in the present case caused by small interstitial-type dislocation loops ('black dot damage') as the dominating obstacles for dislocation glide [25,26].

The apparent inefficiency of helium for hardening at concentrations up to ≈ 0.5 at.% is probably due to its fine dispersion at temperatures below the dissociation temperature of helium–vacancy complexes (≈ 550–650°C for steels). For the limiting case of single helium–vacancy complexes, i.e., He in solid solution, the He-induced strengthening can be estimated by applying the standard equation for solid solution strengthening [27]:

$$\Delta\sigma_{0.2} \approx M\frac{\mu c_{He}^{1/2}\delta^{3/2}}{700}, \tag{1}$$

where $M = 3$ relates the shear stress in a slip plane to the tensile stress in a polycrystal, μ is the shear modulus and δ is a parameter characterizing the modulus and size interaction between solute atoms and dislocations. Assuming $\delta = 1$ as a typical value [28], $\mu = 8 \times 10^{10}$ Pa and $c_{He} = 5 \times 10^{-3}$, Eq. (1) yields $\Delta\sigma_{0.2} \approx 25$ MPa, which is indeed less than an order of magnitude of the observed $\Delta\sigma_{0.2}$ values for both the Manet and the 316 L steel. The corresponding increase in hardness of less than 0.1 GPa would not be detectable as only the major defect types will contribute significantly to hardness increase, according to the generally used superposition law [25].

For higher doses and helium concentrations, the nanohardness of the F82H mod steel keeps increasing, from $\Delta HN = 1.65 \pm 0.62$ GPa after 5 dpa/0.1 at.% He to 2.56 ± 0.56 GPa after 50 dpa/1 at.% He (Fig. 5). Without microstructural information, the following discussion on this further hardness increase of 0.9 GPa remains rather speculative.

This further increase may arise on the one hand from the dislocation network which develops to a saturation after doses as high as 50 dpa. The corresponding increase in yield strength was estimated to be $\Delta\sigma_{0.2} \approx 200$ MPa [25], which would contribute to an increase in hardness of $\Delta H \approx 0.6$ GPa.

On the other hand, the contribution of precipitates or helium bubbles to hardening can be estimated to be [25]

$$\Delta\sigma_{0.2} \approx M\alpha\mu b(Nd)^{1/2}, \tag{2}$$

where α is the strength of the considered obstacle, b is the Burgers vector of the moving dislocation, N is the number density of the obstacles, and d is their size.

Small chromium-rich precipitates are indeed found in the Manet steel [29] and the F82H mod steel [8] after dual-beam irradiations to 50 dpa and 1 at.% He at temperatures between 450°C and 500°C. At 400°C, only a very weak decomposition is observed, the magnitude of which

should decrease at even lower irradiation temperatures. We can therefore expect that the contribution of radiation-induced precipitates to hardening is negligible at temperatures lower than 400°C.

One F82H mod specimen was implanted with 10 at.% He at 250°C with an implantation rate of 5 appm/s. The number density of the formed helium bubbles could be determined very accurately from electron diffraction patterns to $N = 1.25 \times 10^{25}$ m^{-3}, while the bubble diameter was estimated to be $d \approx 2.5$ nm [30]. Small helium bubbles have also been observed in austenitic and ferritic–martensitic steels containing 1 at.% He at temperatures lower than 350°C [23]. A crude estimate of the corresponding increase in hardness with Eq. (2) gives ΔH values greater than 1 GPa, which indicates that helium might contribute to hardening if precipitated into bubbles, e.g., by loop punching above a threshold concentration of around 1 at.%.

5. Conclusions

For helium concentrations up to 0.5 at.%, the observed increases in strength and hardness can be fully attributed to displacement-induced defects (Figs. 3, 5, 9 and 10). Here the helium is believed to reside in very small complexes containing only a few He atoms and vacancies which contribute only negligibly to hardening. The results of the present simulation experiments therefore suggest that helium should have little influence on the mechanical properties of target components for at least 6 months of full power ESS operation which is the time needed to accumulate about 0.5 at.% He. This conclusion must of course be confirmed by mechanical tests on specimens irradiated in real spallation environments and a comprehensive international programme for irradiations in the spallation sources in Los Alamos National Laboratory, USA, and Paul Scherrer Institut, Switzerland, has been established [31].

For helium concentrations above ≈ 0.5 at.%, a preliminary analysis indicates that helium might begin to contribute to hardening. The increase of hardness after helium implantation of 1 at.% is however relatively moderate. Transmission electron microscopy is planned to investigate (a) the structure of the helium bubbles which are assumed to appear after reaching a threshold concentration in the vicinity of 1 at.%, (b) the influence of the implantation rate on the density and topology of the helium bubbles and (c) the interaction of He with the displacement-induced microstructure.

References

[1] H. Lengeler, in: Proc. Meetings ICANS-XIII and ESS-PM 4, PSI Proc. 95-02, Paul Scherrer Institut, Villigen, CH (Nov. 1995) p. 819.
[2] H. Ullmaier, F. Carsughi, Nucl. Instrum. Meth. B101 (1995) 406.
[3] T.A. Gabriel et al., in: Proc. Symp. on the Savannah River Accelerator Project and Complementary Spallation Neutron Sources, University of South Carolina, Columbia, SC, USA (May 1996), to be published.
[4] F. Carsughi, H. Derz, S. Maloy, G. Pott, W.F. Sommer, H. Ullmaier, M. Zaslawsky, to be published.
[5] K. Anderko, K. Ehrlich, L. Schaefer, M. Schirra, KfK-5060, Karlsruhe (1993).
[6] D.R. Harries, J.M. Dupouy, C.H. Wu, J. Nucl. Mater. 133& 134 (1995) 25.
[7] P. Jung, A. Hishinuma, G.E. Lucas, H. Ullmaier, J. Nucl. Mater. 232 (1996) 186.
[8] N. Wanderka, E. Camus, H. Wollenberger, Mater. Res. Soc. Symp. Proc. 439 (1997) 451.
[9] B.N. Lucas, private communication.
[10] U. Stamm, H. Schroeder, J. Nucl. Mater. 155–157 (1988) 1059.
[11] K.K. Bae, K. Ehrlich, A. Möslang, J. Nucl. Mater. 191–194 (1992) 905.
[12] P. Marmy, M. Victoria, J. Nucl. Mater. 191–194 (1992) 862.
[13] J. Chen, P. Jung, J. Nucl. Mater. 212–215 (1994) 559.
[14] H. Schroeder, W. Liu, J. Nucl. Mater. 191–194 (1992) 776.
[15] J.E. Pawel-Robertson, I. Ioka, A.F. Rowcliffe, M.L. Grossbeck, S. Jitsukawa, in: 18th Int. Symp. ASTM STP 1325, ed. R.K. Nastad, M.L. Hamilton, F.A. Garner and A.S. Kumar (American Society for Testing and Materials, Philadelphia, PA, 1997) p. 225.
[16] J.D. Elen, P. Fenici, J. Nucl. Mater. 191–194 (1992) 766.
[17] H. Ullmaier, H. Trinkaus, Materials Science Forum, Vols. 97–99 (TransTech, Aedermannsdorf, 1992) p. 451.
[18] J. Kjems, The European Spallation Source Study, final report, Vol. 3, ch. 4, Risø Nat. Lab., Roskilde, Denmark, ISBN 0902376659, Mar. 1997, pp. 4–24.
[19] D.S. Gelles, J. Nucl. Mater. 149 (1987) 192.
[20] R.L. Klueh, D.J. Alexander, J. Nucl. Mater. 212–215 (1994) 736.
[21] R.L. Klueh, D.J. Alexander, J. Nucl. Mater. 233–237 (1996) 336.
[22] R. Stoller, P. Rice, private communication (1997).
[23] E.H. Lee, G.R. Rao, L.K. Mansur, private communication (1997).
[24] P. Fielitz, PhD thesis, Technical University Berlin (1997); P. Fielitz, M.-P. Macht, V. Naundorf, H. Wollenberger, these Proceedings, p. 123.
[25] G.E. Lucas, J. Nucl. Mater. 206 (1993) 287.
[26] G.R. Odette, G.E. Lucas, J. Nucl. Mater., submitted.
[27] R.L. Fleischer, in: The Strengthening of Metals, ed. D.M. Peckner (Reinhold, New York, 1964) p. 93.
[28] T.H. Courtney, Mechanical Behavior of Materials (McGraw-Hill, New York, 1990) p. 180.
[29] N. Wanderka, E. Camus, V. Naundorf, C. Keilonat, S. Welzel, H. Wollenberger, J. Nucl. Mater. 228 (1996) 77.
[30] E. Camus, N. Wanderka, H. Wollenberger, 126th TMS Annual Meeting, Orlando, Fl, Feb. 9–13, 1997.
[31] Y. Dai, W.F. Sommer, private communication.